Composite Structures 193 (2018) 154–164

Contents lists available at ScienceDirect

Composite Structures

journal homepage: www.elsevier.com/locate/compstruct

Flexural creep tests and long-term mechanical behavior of fiber-reinforced polymeric composite tubes

Zengqin Yang[a], Hui Wang[b], Xiaofei Ma[b], Fulin Shang[a,*], Yu Ma[a], Zhenwei Shao[a], Demen Hou[a]

[a] State Key Laboratory for Strength and Vibration of Mechanical Structures, Xi'an Jiaotong University, Xi'an 710049, China
[b] Xi'an Institute of Space Radio Technology, Xi'an 710100, China

ARTICLE INFO

Keywords:
Polymer matrix composites
Creep deformation
Flexural strength
Mechanical behavior

ABSTRACT

An experimental investigation of the long-term creep behavior of fiber reinforced polymeric composite tubes subjected to flexural loading was performed. The tubes were first tested under a three-point bending scheme at room temperature to determine the ultimate flexural strength (UFS) and to identify the characteristic failure mode and possible failure locations. Creep tests were then carried out at stress levels of 45%, 55%, 65%, and 75% of the UFS at constant temperatures ranging from −60 °C to 100 °C for 500 h, and strain measurements over time were recorded. The tubes were further tested at varying temperatures by applying 22.5 thermal cycles between −60 °C and 100 °C and 9.5 thermal cycles between −160 °C and 80 °C. Similar flexural loads were applied simultaneously on the tubes. Long-term creep deformation of the tube was evaluated using the time-temperature-stress superposition principle, the derived creep main curves, and the Findley model. Finally, the creep deformation and mechanical strength of the tube at expected service conditions over its entire lifetime were predicted.

1. Introduction

Fiber-reinforced polymeric (FRP) composites are increasingly used in the aerospace industry, e.g., in space satellite antennae. Typically, these kinds of structural elements are exposed to environmental conditions such as high and low temperatures, or cyclic variations of temperature. To fulfill the requirements of deep space exploration, the elements need to carry certain mechanical loads under rather wide temperature variations and operate for long durations, typically more than ten years. Naturally, their short-term and long-term durability and structural integrity are of great concern. According to contemporary research from Scott and Lai [1], Narin [2], Fllyin and Rohrbacher [3], Sanders [4], Ray [5], Sethi, and Ray [6], FRP composites, such as carbon fiber and epoxy matrix composites, are sensitive to temperature variations [7] and their mechanical behavior is strongly influenced by temperature [5]. Exposure to low temperatures may cause a plastic to become brittle, which may induce cracking and a propensity to fracture. Exposure to elevated temperatures can result in degradation of mechanical properties, cracking, chalking, and flaking of polymers. Cyclic exposure could cause interfacial debonding and matrix cracking in the composites [8], further degrading the mechanical properties of FRP. For example, Shin et al. [9] reported a sharp reduction of matrix dominant properties such as transverse flexural strength and transverse tensile strength with thermal cycling; this has been recognized as one of the weaknesses of polymer matrix composites during thermal cycling [10].

Another important factor is the time-dependent behavior of the composite as polymeric-based composite materials are viscoelastic in nature. Specifically, stress relaxation or creep deformation will occur when a viscoelastic material is exposed to quasi-static loads and load changes. This time-dependent behavior can be significantly influenced by environmental conditions such as temperature, mechanical loads, or some combination of both. As an example, the application temperature for composite elements made of FRPs is normally below the glass transition temperature of its matrix as the properties of the composite will degrade significantly above this particular temperature. Such viscoelastic effects make it imperative that the time-dependent behavior of these materials be accounted for in the structural design and ground tests of the FRP elements used in space antennae.

The main requirements considered here are that large creep deformation should be avoided and the mechanical strength tolerance should not be exceeded when the elements are tested under the long-term loading conditions encountered during the design life. Two approaches can be taken to analyze the creep deformation and assess the long-term performance of the FRP composite elements. Experimental measurement of the creep strain is straightforward, although testing

* Corresponding author.
E-mail address: shangfl@mail.xjtu.edu.cn (F. Shang).

https://doi.org/10.1016/j.compstruct.2018.03.083
Received 7 September 2017; Received in revised form 30 January 2018; Accepted 21 March 2018
Available online 22 March 2018
0263-8223/ © 2018 Elsevier Ltd. All rights reserved.

facilities are required, testing time may be long, and the financial costs could be high. Numerical calculation of the creep strain profiles using linear or nonlinear viscoelastic models may be efficient in terms of difficulty and cost. Because FRP composites often show direction dependent properties the anisotropy must be considered. Additionally, composites are naturally inhomogeneous and their mechanical behavior is related to both its constituents and the interface between the fiber and matrix. Development of a constitutive model for composite materials with such strong anisotropy and inhomogeneity is difficult, although not impossible. For example, recent work by Pettermann and Desimone [11] implemented a constitutive material law for linear thermo-viscoelasticity in the time domain that considered the full anisotropy of the time-dependent relaxation formulation, including the elastic and the viscous properties into the ABAQUS finite element code. However, there are a number of theoretical assumptions embedded in these kinds of models, and they might not fully represent real composite materials.

Another critical issue for numerical models is that the validity of the extrapolation of coupon material creep data to larger structural elements remains uncertain, and this could further complicate any theoretical or numerical analyses. McClure and Mohammadi [12] examined the compressive creep behavior of thermoset pultruded fiberglass-reinforced-plastic angle sections and concluded that there was no real benefit in carrying out detailed creep investigations on full-sized members. According to the authors' understanding, however, there is no guarantee that one can simply replace the creep or viscoelastic behavior of a composite structural element with a theoretical prediction based merely on experimental data of composite material coupons. It is often true that mechanical properties determined from FRP coupons cannot be extended homothetically to a bigger scale because of the microstructure of the two phases composing the material. It is quite possible that the stress state will vary over time because of stress redistributions within the elements. In practice, manufacturers often do not provide the composition of their composite materials, including the amount and direction of fibers. This makes any analysis more difficult.

From the above arguments, it is still reasonable and technically acceptable to experimentally test the creep behavior of composite elements and make theoretical analyses based on the obtained data. The creep of FRP composites, concerning both stiffness and strength, needs to be taken into account in their design and safety assessment, which are relevant to their structural performance after being manufactured. In fact, available design and analysis recommendation or prospective guidelines for the consideration of creep effects for FRP structures are somewhat limited. This may become a barrier for corresponding engineering design and assessment.

The creep of FRP composites has been the subject of extensive research during the last thirty years, as summarized in [1,13]. Several studies concerning the creep behavior of FRP elements or structures have been performed. MacClure and Mohammadi [12] performed compression creep tests of GFRP angle stubs under constant environmental conditions at a stress level equal to 45% of the buckling load for over 2500 h. Scott and Zureick [14] performed compression creep tests of a vinylester and E-glass composite sheet for durations up to 10000 h, with loads from 20% to 60% of the failure load. Shao and Shanmugam [15] tested flange beams made of isophthalic polyester matrix reinforced by E-glass fibers using a three-point bending setup at 25% and 50% of the maximum static load. However, these experiments were performed without precise control of the ambient conditions such as temperature and humidity.

Petermann and Schulte [16] tested carbon fiber reinforced epoxy HTA (12 K)/6376 laminates having a symmetric $(\pm 45)_{2S}$ layup at room temperature and seven stress levels ranging between 40% and 86% of the ultimate tensile strength, for about 120 h. They introduced a power law function to model the creep deformation, and estimated the long-term damage evolution induced by creep and fatigue and the endurance limit. Goertzen and Kessler [17] studied the creep behavior of a carbon fiber and epoxy matrix composite with room temperature tensile creep and elevated temperature flexural creep experiments. The stress levels for the tensile creep tests were 65% and 77% of the ultimate tensile strength. The flexural tests were done at ten constant temperatures between 30 °C and 75 °C, and creep recovery cycles were adopted following isothermal creep tests. Ascione et al. [18] developed an experimental setup to creep test GFRP laminates and their constituents (i.e., the matrix and the fibers) at a constant temperature of 20 °C. Mancusi et al. [19] performed creep tests on FRP-strengthened beams at a constant temperature under a pure bending state by applying constant external loads. They further examined the buckling behavior of FRP thin-walled beams and columns, and considered both local and global buckling of these components and their influence on the failure loads [20,21]. Bottoni et al. [22] performed 760-days-long tests on GFRP specimens subjected to traction and shear forces at 20 °C and relative humidity of 60% inside a climate room. Their specimens were cut from plates, flanges, and webs of GFRP beams. Boscato et al. [23] tested two open-section GFRP beams subjected to a constant load for about one year, and evaluated the long-term deformation, the residual deflection after unloading, and the influence of creep strains on the flexural torsional buckling phenomenon. Yanes-Armas et al. [24] investigated GFRP-polyurethane web-core sandwich structures subjected to sustained loading and assessed their long-term structural performance, with an emphasis on creep of both FRP and polymeric foam constituent materials. These studies mainly focused on the creep deformation analysis of composite materials and structures at constant temperatures, while their mechanical behavior under cyclic thermal and mechanical loads was less discussed.

In this paper, creep tests were performed on an FRP tube under short-term isothermal conditions ranging from −60 °C to 100 °C, and under cyclic thermal conditions between −60 and 100 °C and −160–80 °C. Based on the experimental data obtained, the long-term creep deformation, mechanical performance, and service reliability after the 12-year design life were assessed.

2. Static bending tests

FRP composite tubes with a ply stacking sequence of [15/−15/0/90/0/−15/15] were made from BS-2 epoxy resin and M40JB carbon fiber supplied by CAST Corporation. The nominal inner diameter of the tube was 24 mm and its wall thickness ranged from 0.65 mm to 0.8 mm. The tubes were cut from tubes employed in real applications, and were about one-third the length of the original tube (i.e. 600–800 mm).

The FRP tube was subjected to a static bending moment to mimic the realistic working load. To determine its deformation characteristics, flexural modulus, and flexural strength, static bending tests were conducted at room temperature. Fig. 1 shows the three-point bending fixture and measurement devices, with a reference to technical standards GB/T 1456-2005 [25] and GB/T 1449-2005 [26]. The load was applied to the middle of the upper surface of the tube. Arc-shaped indenter and supports were used (Fig. 1b) to avoid local collapse or introducing any damage to the tube surface due to stress concentrations during loading. To understand the overall mechanical properties of the tube at different cross-sections, nine strain rosettes (AVIC Type BA350-2BB150) were arranged to measure the strain during loading, as shown in Fig. 1c. Five were close to the middle of the tube to monitor the possible failure positions. Eight were symmetric relative to the axial middle plane. All strain gauges recorded variations of the axial (longitudinal) and circumferential (transverse) strains. Clock gauges were attached to the middle bottom surface and the end sections of the tube as an auxiliary means to measure the global bending deformation. The multiple-step loading scheme was applied with a loading rate of 2 mm/min.

Fig. 2a shows one of the typical force-displacement curves at the loading point. A nearly linear relationship between the force and deflection was found before failure. At the failure moment, the force dropped suddenly to zero. The FRP tube samples exhibited brittle

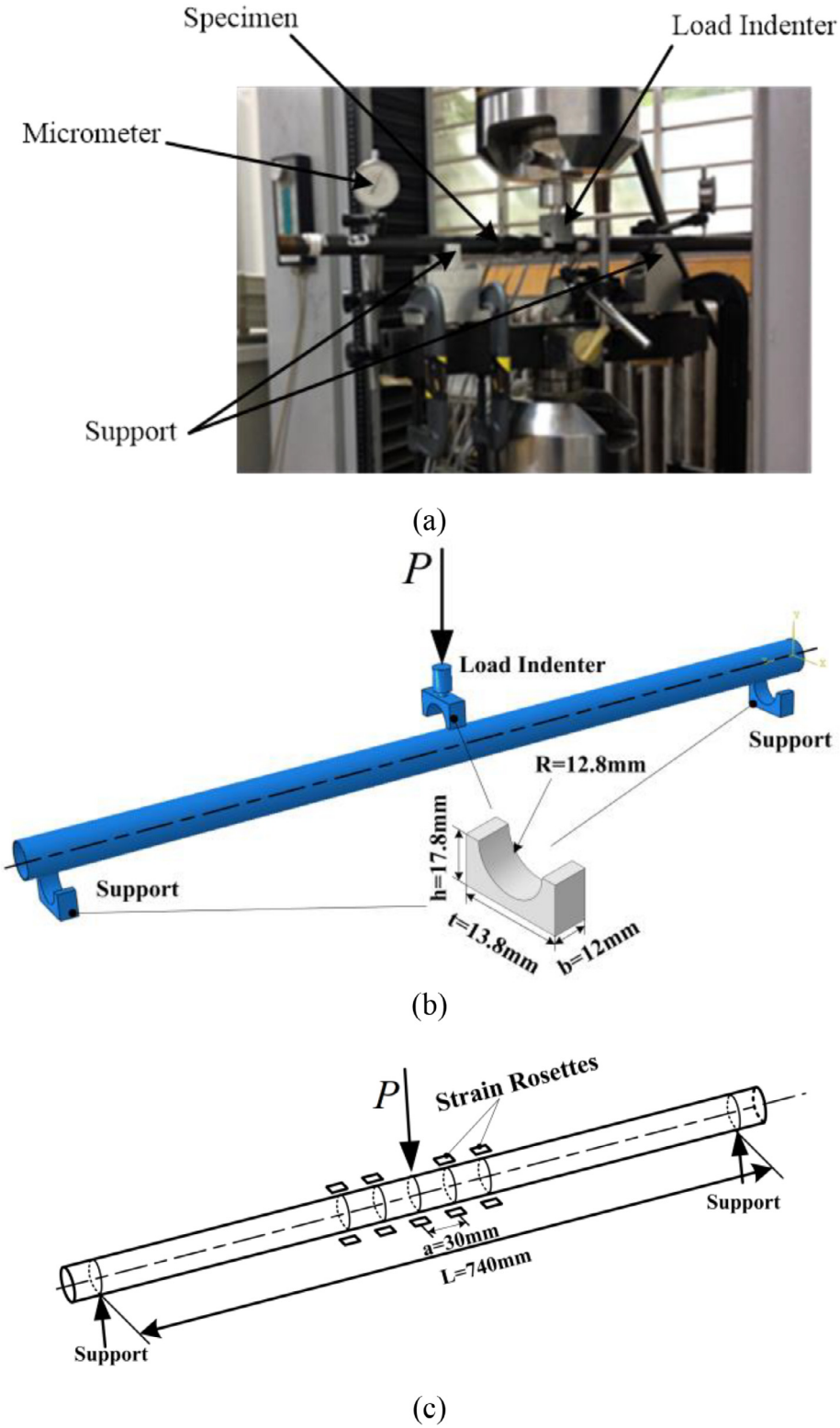

Fig. 1. Static bending test of the FRP tube.

rupture features, and the maximum bending moment was identified as the ultimate flexural load. Fig. 2b shows the typical fracture morphology of the FRP tube after testing. A crack first appeared on the upper surfaces, which were under a compressive stress state, and the fracture surface was relatively flat and normal to the tube axial direction. The crack grew further towards the two side surfaces, and turned its extension direction gradually to 30–45° relative to the tube axis. All the samples tested had similar force-displacement curves and fracture morphologies.

The flexural modulus and the ultimate flexural strength (UFS) of the FRP tube is calculated by using the material mechanics method, i.e.,

$$E = \frac{4Pl^3}{3(D^4-d^4)\pi f} \quad (1)$$

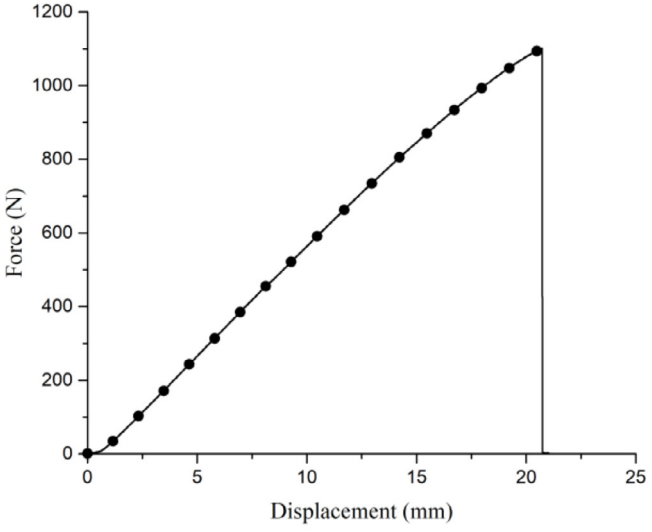

(a)

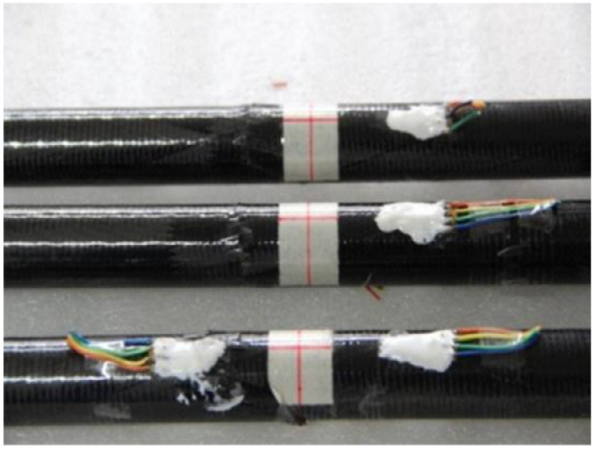

(b)

Fig. 2. Experimental results of the static bending tests. (a) Force-displacement curve and (b) photograph of the fracture morphology.

$$\sigma_C = \frac{8P_C lD}{\pi(D^4 - d^4)} \tag{2}$$

where E is the effective flexural modulus, σ_C is the UFS, P is the bending force, P_C is the maximum bending force, f is the deflection of the loading point, l is the clear span between the two supports, and D and d are the outer and inner diameters of the tube, respectively.

The average effective flexural modulus of all FRP tubes, E, was 137.9 GPa. The UFS, σ_C, was 523.71 MPa, which was the minimum value over all the tubes with a consideration of its service safety.

According to the experimental results, the tube failed because of longitudinal compressive stresses and the failure position was near the middle of the upper surface (about 30 mm away from the loading point). At the critical state, the ultimate strain value at the failure position was $\varepsilon_u = -2924\ \mu\varepsilon$, which can serve as a failure criterion for the FRP tube under bending.

3. Isothermal creep tests

Accelerated creep tests of the tube at typical temperatures were performed inside controlled environmental chambers, including a lower temperature chamber (ACS WS6000C) (Fig. 3a) and a high temperature chamber (HARDY HT323P) (Fig. 3b). Isothermal flexural creep tests were carried out at constant temperatures of −60 °C, −20 °C, 25 °C, 60 °C, and 100 °C. Four samples at each temperature were loaded at four stress levels, roughly equal to 45%, 55%, 65%, or 75% of the UFS of the tube by hanging weights in the middle of the tube along the transverse direction (see Fig. 3). Two sets of tests were done to check the repeatability of the experimental results. Isothermal creep tests were performed for over 500 h, with a reference to technical specifications of MIL-HDBK-17-1F [27] and GB/T 11546.1-2008 [28].

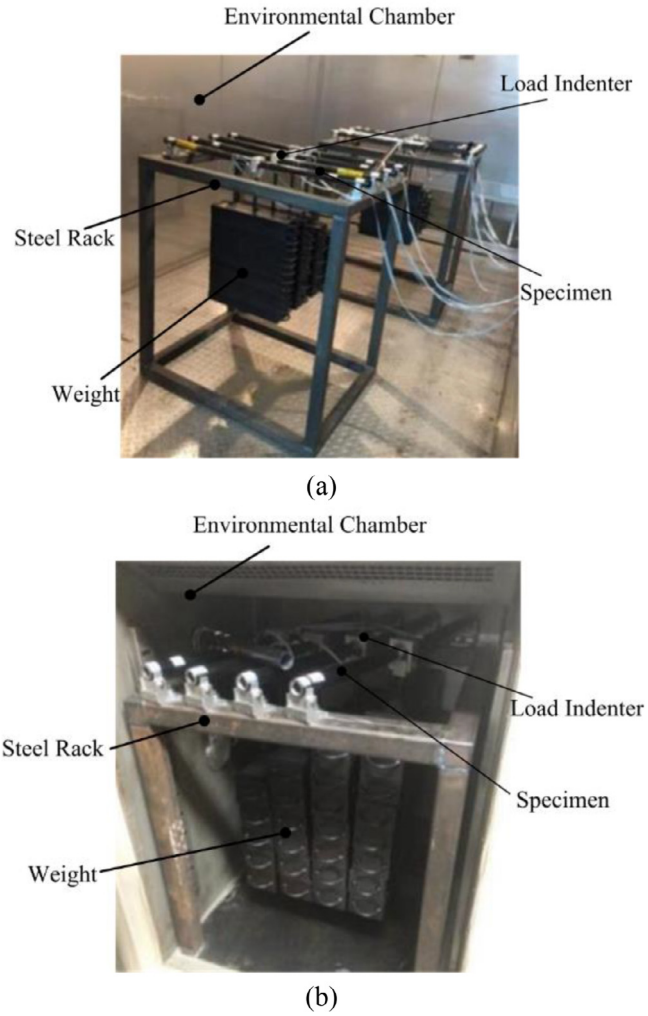

Fig. 3. Isothermal creep testing chamber. (a) Lower temperature chamber (ACS WS6000C) and (b) higher temperature chamber (HARDY HT323P).

Fig. 4 is a schematic plot of the isothermal creep test, where the labels show the locations of the strain rosettes. Strain gauges (KYOWA KFRP-2-120-CA-1) were arranged along both longitudinal and transverse directions at each point. Fig. 5 shows the creep strains at different

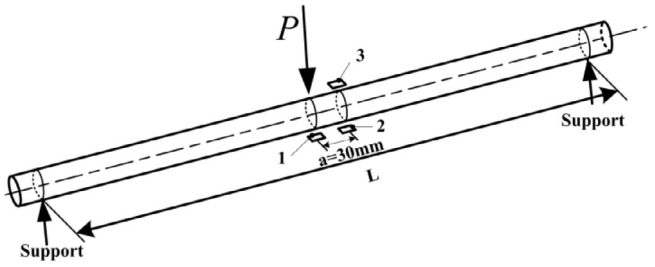

Fig. 4. Schematic of the isothermal creep testing method.

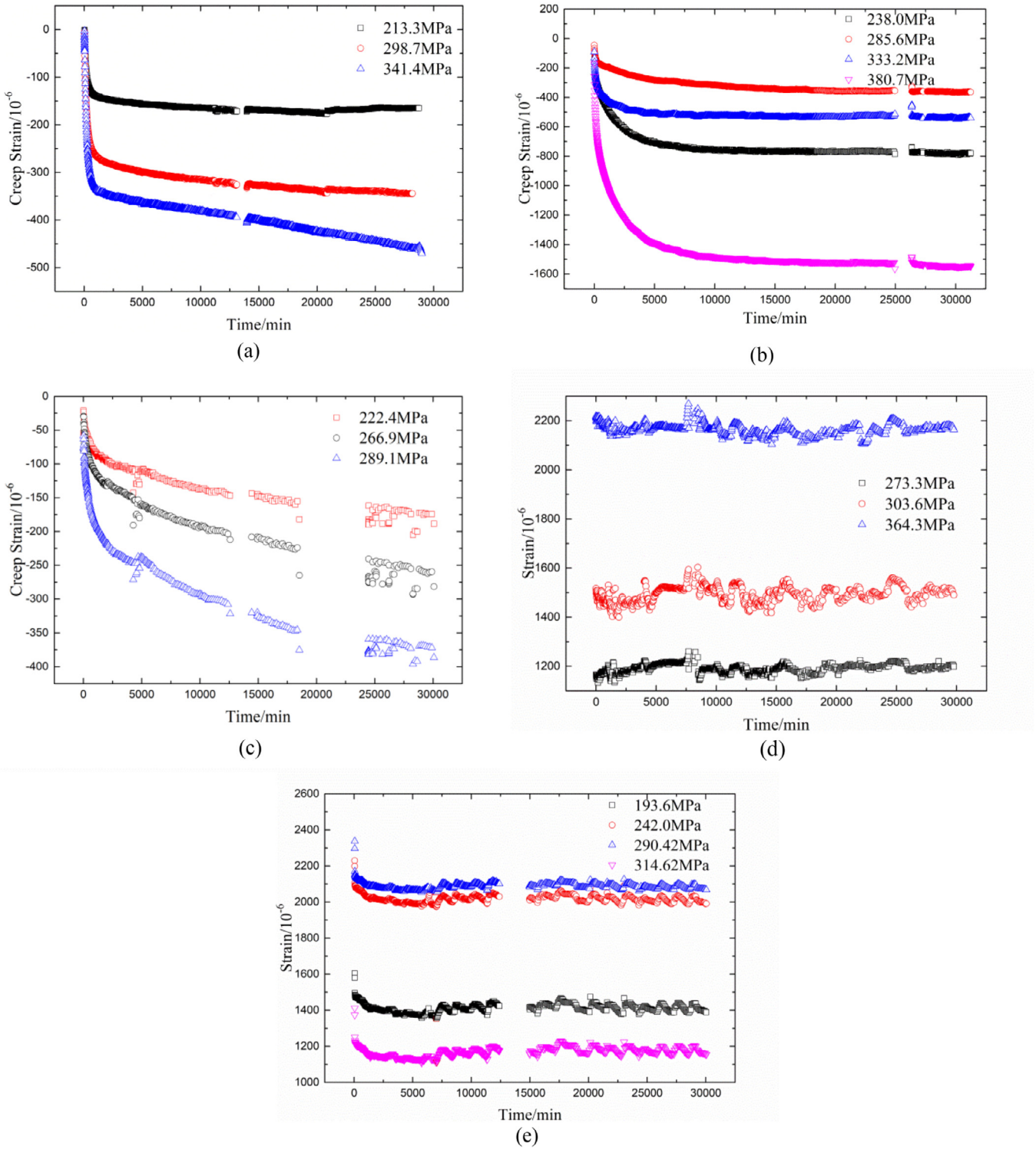

Fig. 5. Experimental creep test results. (a) Longitudinal creep strain at gauge point No. 3 at 25 °C, (b) transverse creep strain at gauge point No. 1 at 60 °C, (c) longitudinal creep strain at gauge point No. 3 at 100 °C, (d) longitudinal strain at gauge point No. 1 at −20 °C, and (e) longitudinal strain at gauge point No. 1 at −60 °C.

temperatures over time at gauge points No. 1 and No. 3. Gauge point No. 3 was very close to the initial fracture position of the tube found during static bending tests. The creep deformation of the FRP tubes in the temperature range from 25 °C to 100 °C (Fig. 5a–c) manifested the instantaneous (first) creep and steady (second) creep stages, but the accelerated (third) creep stage did not emerge. The steady creep period was relatively long compared with the instantaneous stage, which is in accordance with the typical creep features of many polymer matrix composites. Additionally, the creep strain rate increased with increasing stress levels at a given temperature. Fig. 5d and e show the longitudinal strain at −20 °C and −60 °C, respectively. There is no clear evidence of instantaneous, steady, and accelerated creep stages. In particular, after deformation fluctuations in the initial period, the tubes had nearly constant strain amplitude over time. These results

demonstrate that the typical creep temperature range of this composite tube is around 25–100 °C, and the tube does not creep at temperatures lower than −20 °C. These observations are consistent with the creep characteristics of polymer matrix composites with similar constituents [17].

4. Thermal cyclic creep tests

As mentioned in the Introduction, the FRP tubes often experience the space environmental conditions with a wide temperature change, say between −160 °C and 100 °C, and need to run for a long duration. Therefore, it is necessary to characterize their deformation under thermal cyclic condition together with the application of certain mechanical loads. The induced strain in viscoelastic FRP materials may have elastic, viscous, and thermal components. The viscous (i.e., creep) strain is the most difficult one to calculate. By definition, creep is the time-dependent deformation of a material under constant load. In this work, thermal cyclic creep tests were devised to measure the creep strain when the tube undergoes thermal cyclic loading conditions. Thermal cyclic tests between −60 °C and 100 °C and between −160 °C and 80 °C were performed to simulate the real environmental conditions under which the tube will be used.

Thermal cyclic tests at −60–100 °C were performed by employing an ACS WS6000C chamber (Fig. 3a). Fig. 6a shows the diagram of the thermal cyclic test procedure. The holding periods at the maximum and minimum temperatures were two hours and the rate of temperature change was 3 °C/min. RH of 48% was maintained throughout the tests. This test was repeated for 25.5 thermal cycles, according to technical requirements. The loading method and the arrangement of the strain gauges were the same as those of the isothermal creep test.

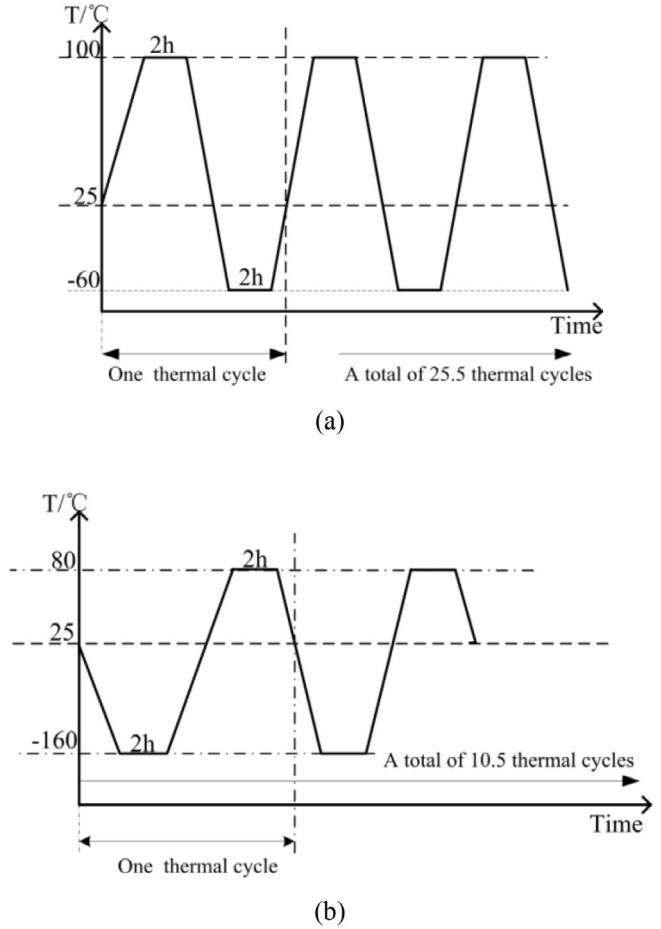

Fig. 6. Diagram of the thermal cyclic procedure. (a) −60–100 °C and (b) −160–80 °C.

Fig. 6b is the diagram of the thermal cyclic procedure used for the −160–80 °C creep tests. The rate of temperature change was 3 °C/min, the holding times at the maximum and minimum temperatures were two hours, and the number of total thermal cycles was 9.5. Fig. 7a depicts the arrangement of the strain gauges, which was slightly different than the previous arrangement, considering the possible failure locations of the tubes under this particular condition. A constant load was implemented using a force control system with a load resolution of 1% (see Fig. 7b).

Fig. 8a displays the experimental results of the −60–100 °C thermal cycling tests when the tubes were subjected to stress levels between 195.3 MPa and 334.8 MPa. Cyclic variations in the strain amplitude are evident, which is a typical feature for thermal strain. Furthermore, the creep deformation at higher temperatures (e.g., 100 °C) increased slightly, while the creep deformation at lower temperatures (e.g., −60 °C) was nearly unchanged. Results also confirmed that creep deformation only takes place at relatively high temperatures. Finally, the strain amplitudes increased with increasing stress levels, which is certainly true for the elastic response of the elements.

Fig. 8b shows the longitudinal strain variations of the FRP tube at gauge point No. 2, which is near the failure point of the tube, at stress levels of 120 MPa, 200 MPa, and 250 MPa. The strain exhibited periodic fluctuations with the temperature change between −160 °C and 80 °C. The absolute values of the strains increased similarly with increasing stress levels. The creep deformation of the tubes during the higher temperature holding period is noticeable. The deformation of the tubes during the lower temperature holding period again shows no typical creep features. Compared with the deformations at the higher temperature period, the tubes tended to creep slightly, but not as much as during the −60–100 °C thermal cycling case. In addition, the strain amplitude fluctuations were greater than those of the −60–100 °C thermal cycling case.

5. Prediction of long-term creep deformation of the FRP tube

Theoretical models are required to predict the long-term behavior of the composites using the short-term creep data obtained experimentally. Commonly accepted and widely used models include the time-temperature-stress superposition principle, the Findley model, and the creep master curve [29–34].

5.1. Creep master curve method

The creep master curve method is based on the principles of time-temperature and time-stress superposition of the viscoelastic behavior of a resin matrix. According to the time-temperature superposition principle, the creep compliance curve of the material at different temperatures can be shifted by an appropriate temperature shift factor to form the corresponding master curve at a reference temperature. Using the master curve at the reference temperature, initial predictions of compliance levels for a composite structure operating under constant load at the reference temperature of interest are possible. The composite material is assumed to be linear viscoelastic. Furthermore, as the flexural compliance of the material in question is different from its compliance in tension, the ratio of the flexural compliance to the tensile compliance is also assumed to be constant.

Fig. 9 shows the time-temperature superposition principle. The long-term creep compliance curve $S(T_{\text{ref}},t)$ at a reference temperature T_{ref} can be constructed by shifting the short-term compliance curve at other temperatures along the logarithmic time axis through a time-temperature shift factor $\log\phi_T$, which is given by

$$S(T_{\text{ref}},t) = S(T_i,\phi_T t) \tag{3}$$

where $S(T_i,t)$ is the creep compliance curve at temperature T_i, defined as

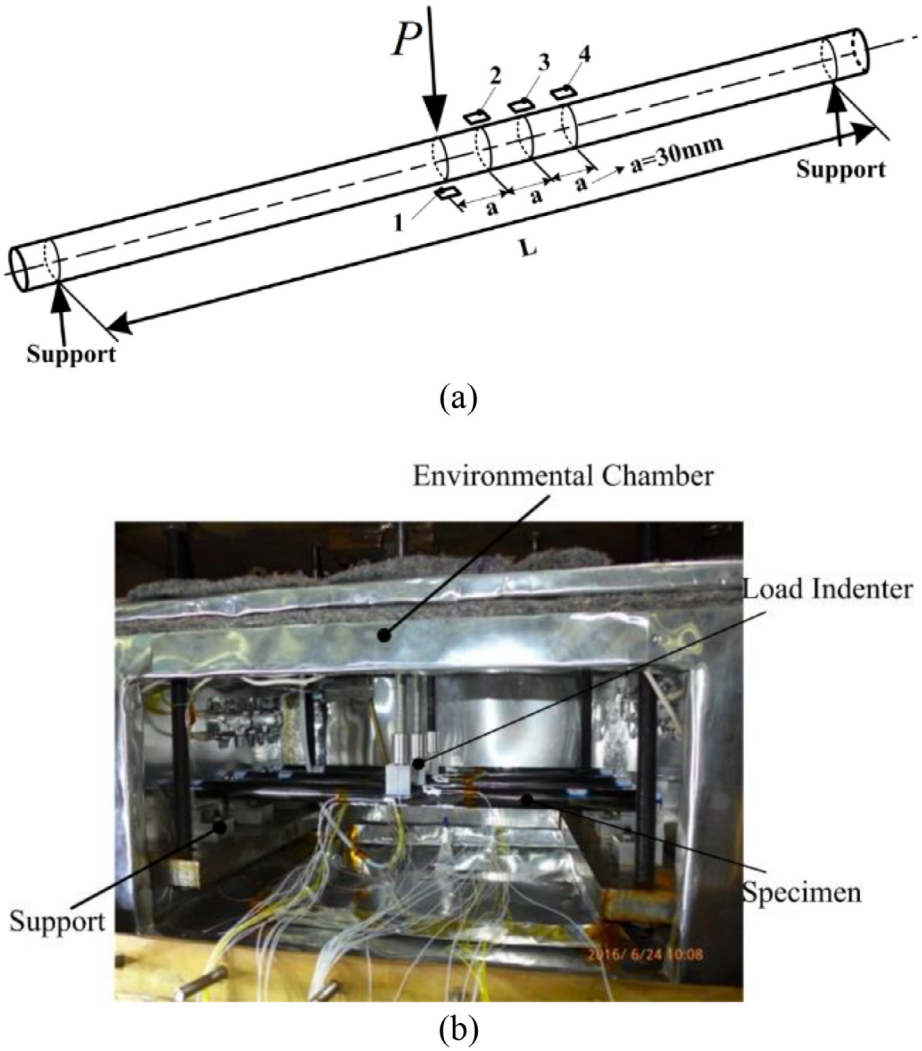

Fig. 7. (a) Measurement method and (b) testing chamber for −160–80 °C thermal cyclic creep tests.

$$S(T_i,t) = \varepsilon(T_i,t)/\sigma \tag{4}$$

where $\varepsilon(T_i,t)$ is the strain at temperature T_i and σ is the constant stress applied.

Similarly, according to the time-stress superposition principle, the long-term creep behavior at lower stress levels can be predicted by using short-term creep data at higher stress levels. The long-term creep compliance curve at a reference stress can be obtained by shifting the short-term compliance curve at other stress levels through a time-stress shift factor $\log\phi_\sigma$.

Thus, by employing the time-temperature-stress superposition principle, the time-temperature-stress shift factor $\log\phi_{T\sigma}$ is given by

$$\log\phi_{T\sigma} = \log\phi_T^{\sigma_{\text{ref}}} + \log\phi_\sigma^{T_{\text{ref}}} \tag{5}$$

where $\log\phi_T^{\sigma_{\text{ref}}}$ is the time-temperature shift factor at the reference stress and $\log\phi_\sigma^{T_{\text{ref}}}$ is the time-stress shift factor at the reference temperature. In this way, the creep behavior of a composite material at a certain temperature and stress level can be determined by the time-temperature shifting under a constant stress case and the time-stress shifting under a constant temperature case.

5.2. Findley model

The phenomenological creep model developed by Findley [34] introduced a mathematical expression to describe the creep behavior of the material, which is more suitable for the prediction of the first and second creep deformation stages. According to this model, the creep response can be divided into time-independent and time-dependent strains. In the case of constant stress, the creep strain can be expressed as

$$\varepsilon(t) = \varepsilon_0 + m\left(\frac{t}{t_0}\right)^n \tag{6}$$

where ε_0 is the initial stress-dependent and time-independent elastic strain, m is a coefficient related to both stress and temperature, and n is a stress-independent and temperature-dependent material constant. The above parameters can be determined by fitting to experimental data.

5.3. Case 1: Long-term creep deformation prediction at 25 °C

Using the theoretical models, the FRP tube creep behavior throughout its design life was predicted based on the creep data obtained from both isothermal and thermal cyclic tests. The longitudinal creep compliance curve of gauge point No. 3 at 25 °C is shown in Fig. 10a. A smooth creep compliance master curve at a reference stress of σ_{ref} = 222.4 MPa was obtained by shifting the creep compliance curve at other stress levels, which also somewhat validates the time-stress superposition principle for the composite tube considered here. The creep compliance master curve at the reference stress σ_{ref} = 222.4 MPa is shown in Fig. 10b.

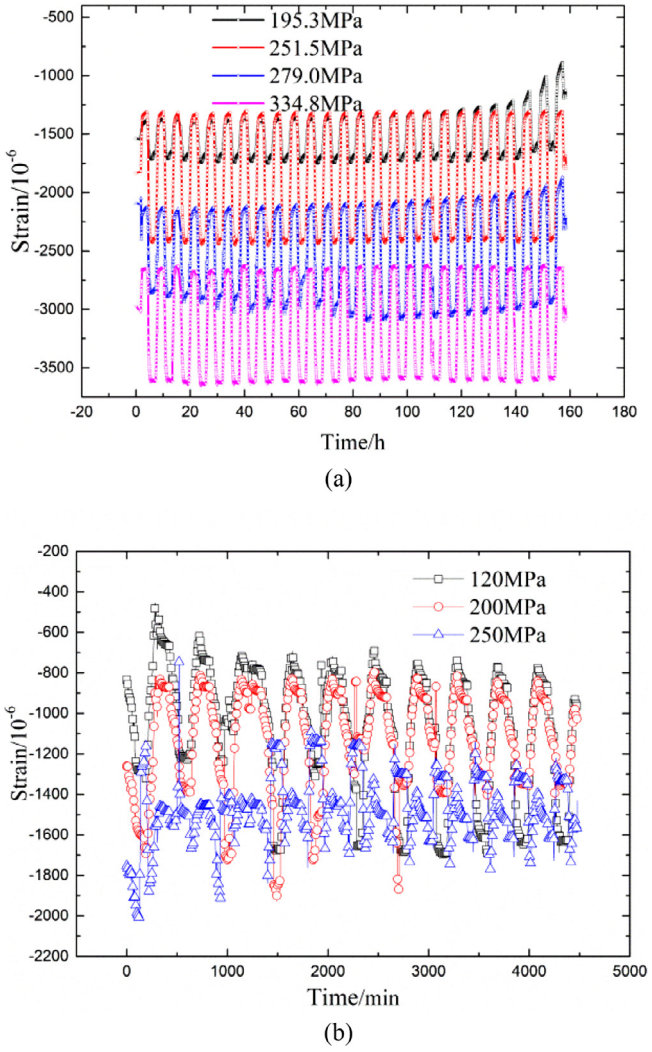

Fig. 8. Longitudinal strain at gauge point No. 2 from thermal cycling tests at (a) −60–100 °C and (b) −160–80 °C.

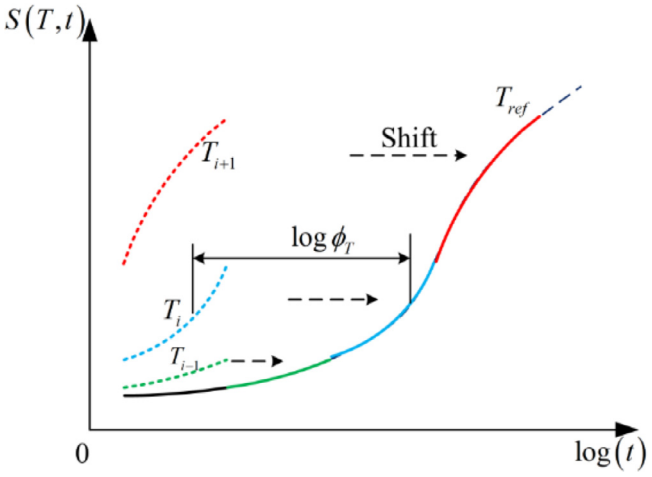

Fig. 9. Illustration of the time-temperature superposition principle.

According to the relationship between the shift factors $\log\phi_\sigma$ at different stress levels, the creep compliance master curve at a lower stress level can be obtained by an interpolation method as well. Fig. 11 shows the creep compliance master curve at a stress level of 100 MPa, which greatly prolonged the duration of the reliable prediction of creep

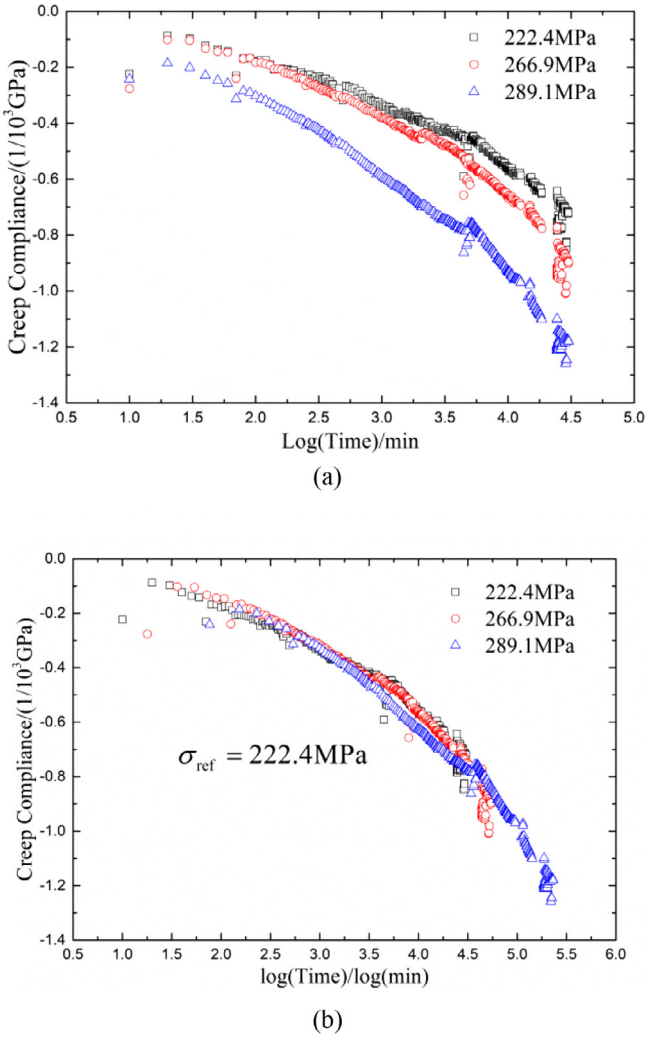

Fig. 10. (a) Longitudinal creep compliance of gauge point No. 3 at 25 °C. (b) Master curve of creep compliance at 222.4 MPa.

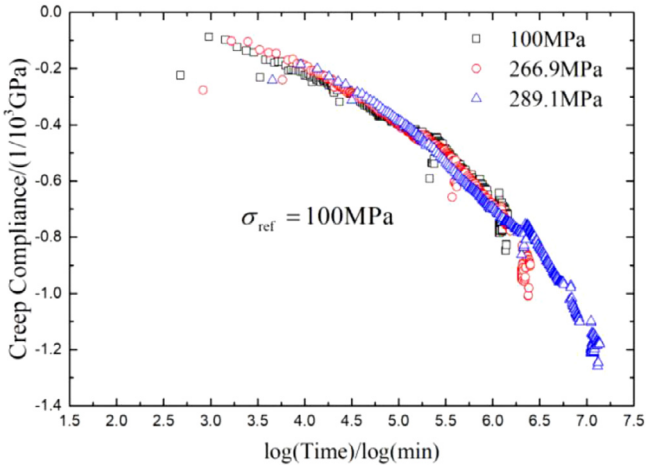

Fig. 11. Longitudinal creep compliance curve and master curve of gauge point No. 3 at 100 MPa.

deformation. For the tube under typical service conditions at 100 MPa after a 12-year design life, the creep strain was estimated to be 99.6 με. The initial elastic strain of the FRP tube measured from the static bending test was 589.9 με. Therefore, the predicted total strain of the tube is 689.5 με at 100 MPa and 25 °C.

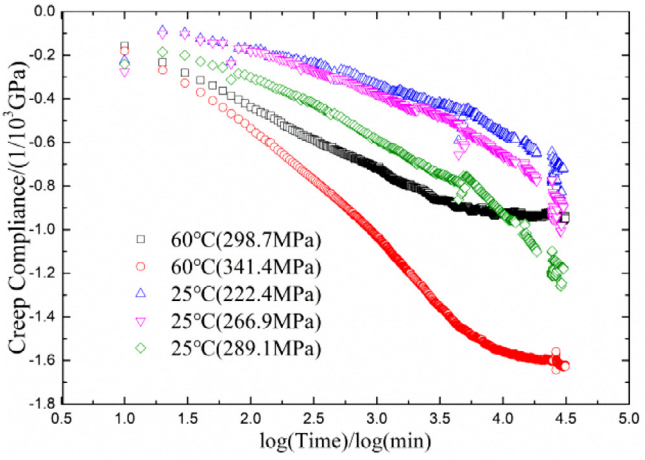

(a)

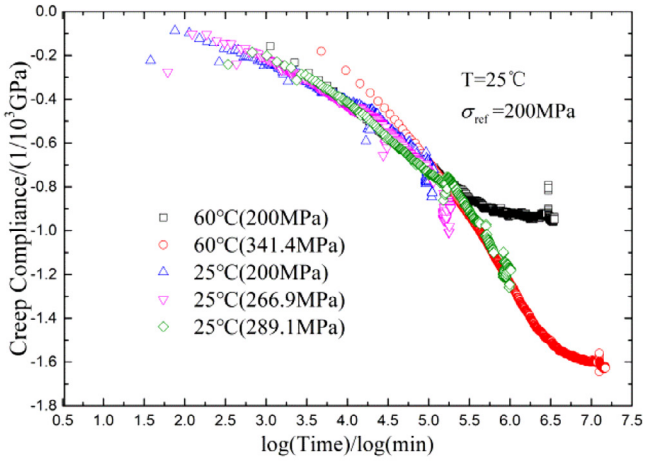

(b)

Fig. 12. (a) Longitudinal creep compliance curve and master curve of gauge point No. 3 at 200 MPa. (b) Master curve of creep compliance at reference conditions.

Fig. 12a shows the longitudinal creep compliance curve at different temperatures and stress levels. The creep compliance master curve at the reference conditions (T_{ref} = 25°C, σ_{ref} = 200 MPa) is given in Fig. 12b. The estimated creep deformation when operating at service conditions for 12 years at the reference conditions is 319.8 με. By superimposing the initial elastic strain of 1274.4 με, the long-term total deformation of the FRP tube at this condition is predicted to be 1594.2 με.

5.4. Case 2: Long-term creep deformation prediction at 100 °C

Because of the limitations of the deformation data at high temperatures, the Findley model was used to predict the long-term creep deformation of the tube at 100 °C. The creep deformation curves at stress levels of 100 MPa and 200 MPa (Fig. 13) were obtained by fitting the model to the measured creep strain data. Based on the Findley model, the creep strain-time curve of the tube at 100 MPa and 100 °C is given by

$$\varepsilon_{cr} = -30.973t^{0.108} \quad (7)$$

and the creep strain-time curve of the tube at 200 MPa and 100 °C is given by

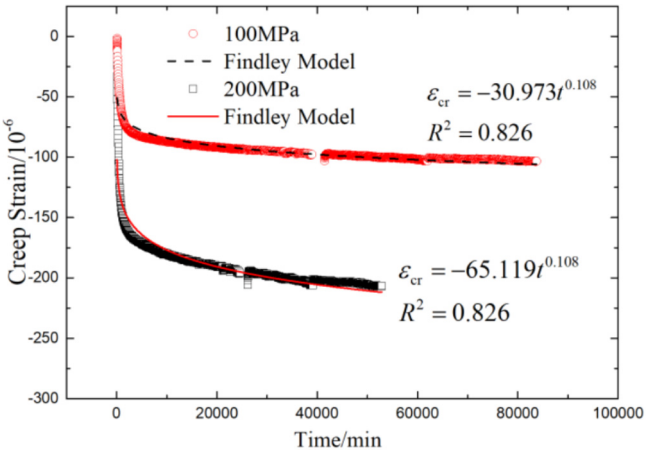

Fig. 13. Creep strain curves of the RFP tube at 100 °C, and 100 MPa or 200 MPa.

$$\varepsilon_{cr} = -65.119t^{0.108}. \quad (8)$$

Using the these expressions, the predicted creep deformations of the FRP tube at 100 MPa and 200 MPa at the end of the 12-year design life are estimated to be 168.0 με and 353.3 με, respectively. Thus, the total predicted deformations at these service conditions are about 757.9 με and 1627.7 με, respectively.

6. Assessment of the mechanical strength of the FRP tube

According to the experimental results of the static bending tests, the tube fractured because of longitudinal compressive failure when its compressive strain reached a critical value $\varepsilon_u = -2924$ με. Based on this failure criterion, the mechanical strength of the FRP tube was assessed.

For the case of constant temperature, the total strain in the tube consists of the initial elastic strain ε_{el} and the creep strain ε_{cr}. Thus, the maximum strain failure condition is given by

$$|\varepsilon_{el} + \varepsilon_{cr}| \leqslant |\varepsilon_u|. \quad (9)$$

In the case of thermal cycling, the total strain in the tube consists of the initial elastic strain ε_{el}, the thermal strain ε_{th}, and the creep strain ε_{cr}, given by

$$\varepsilon = \varepsilon_{el} + \varepsilon_{th} + \varepsilon_{cr}. \quad (10)$$

According to the results of the thermal cyclic tests, the creep deformation had relatively small amplitude and was nearly unchanged during the lower temperature period. Therefore, ignoring the creep strain, the total strain in the tube is a superposition of the initial elastic strain and the thermal strain. Thus the failure condition becomes

$$|\varepsilon_{el} + \varepsilon_{th}| \leqslant |\varepsilon_c| \quad (11)$$

From the results of the −60–100 °C thermal cyclic creep tests, the effective longitudinal thermal expansion coefficient of the FRP tube α_L was calculated to be 3.11 με/°C. The thermal strain was then $|\varepsilon_{th}| = \alpha_L(T - T_{ref}) = 264.4$ με. By superposition of the initial elastic strain of the tube under this condition (1274.4 με), the total deformation is predicted to be about 1525.7 με after 12 years. From the test results of the −160–80 °C thermal cyclic creep tests, the longitudinal thermal expansion coefficient of the FRP tube α_L was 3.11 με/°C. The thermal strain was then $|\varepsilon_{th}| = \alpha_L(T - T_{ref}) = 414.4$ με. Thus, the total deformation of the tube under these conditions may reach 1675.7 με after 12 years.

Using the strain failure criterion, the long-term mechanical strength of the FRP tube was assessed. The flexural compliance S_L at the end of the lifetime can be determined from the deformation of the tube under different service conditions. The initial flexural compliance S_0 of the tube was calculated to be 6.372×10^{-12} Pa^{-1} from the isothermal

Table 1
Mechanical performance of the FRP tube after long-term service under different conditions.

Temperature/°C	Stress/MPa	Total Strain/με	Flexural compliance/$1 \times 10^{-12}\,Pa^{-1}$	Retention ratio of flexural strength/%	Reduction in flexural modulus/%
25	200	−1594.2	7.971	79.9	20.1
100	200	−1627.7	8.139	78.0	22.0
−60 ~ 100	200	−1904.3	9.522	70.0	30.0
−160 ~ 80	200	−1688.8	8.444	75.5	24.5

creep tests and $6.306 \times 10^{-12}\,Pa^{-1}$ from the thermal cyclic tests. By comparing the flexural compliances S_L to S_0, the UFS was determined. Table 1 summarizes the predicted mechanical properties of the FRP tube during its lifetime at different service conditions.

7. Conclusions

Characterization of the mechanical behavior and creep deformation of the FRP composite tube is of critical importance in terms of its long-term deformation and mechanical strength. Based on the experimental static and creep results measured at different stress and temperature levels, this work established the creep master curve and predicted the long-term deformation of the FRP composite tube. The mechanical strength within a 12-year design life was then assessed using a maximum strain failure criterion.

When subjected to a bending moment, the FRP tube tended to fail from a brittle rupture and fracture occurred from axial compressive failure. The crack initiated at the compressive side of the outer surfaces of the tube and the fracture surface was relatively flat and normal to the tube axial direction. The crack grew further towards the two side surfaces, and turned its extension direction gradually to 30–45° relative to the tube axis.

Isothermal creep tests and thermal cyclic tests indicated that the FRP tube exhibited typical creep characteristic when the operating temperature ranged from 25 °C to 100 °C, and the creep rate increased with increasing stress and temperature levels. The creep curves included the instantaneous and steady creep stages at the expected service conditions, without an emergence of the accelerated creep stage.

To predict the long-term creep deformation, the master creep compliance curve of the tube at 25 °C was determined using the time-temperature-stress superposition principle. The creep deformation at 100 °C was predicted using the Findley model. The mechanical performance of the tube at different temperatures and stress levels throughout its lifetime was evaluated using the maximum strain criterion. The long-term deformation of the tube at the typical service conditions will not exceed the ultimate flexural strain, and the tube therefore meets the requirement of mechanical strength. The reduction in flexural modulus over the 12-year design life ranges from 20.1% at 25 °C to 30% when experiencing thermal cyclic conditions between −60 and 100 °C. The stress levels inducing failure after 12 years will reduce the UFS to 70% of its initial value at −60–100 °C and to 80% of its initial value at 25 °C.

One more noteworthy observation is that some of the tested tubes failed abruptly during the −160–80 °C thermal cycling under a bending stress higher than 250 MPa. This might be related to a ductile–brittle transition or a cryogenic property of the polymeric composite materials, and needs to be further investigated in the future.

Acknowledgments

The authors would like to acknowledge Xi'an Institute of Space Radio Technology for providing specimens and financial support. The authors are also grateful to Prof. Hongbin Geng and Dr. Gang Lv from the School of Materials Science and Engineering at the Harbin Institute of Technology for the use of testing equipment and technical advice. We thank Melissa Gibbons, PhD, from Liwen Bianji, Edanz Editing China (www.liwenbianji.cn/ac), for editing the English text of a draft of this manuscript. This work was partially supported by the National Natural Science Foundation of China through Grants No. 11672220 and No. U1537213.

References

[1] Scott DW, Lai JS, Zureick AH. Creep behavior of fiber-reinforced polymeric composites: a review of the technical literature. J Reinf Plast Compos 1995;4(6):588–617. http://dx.doi.org/10.1177/073168449501400603.
[2] Nairn JA. Matrix microcracking in composites. In: Kelly A, Zweben C, editors. Comprehensive composite materials 2000;2:403–432, Elsevier, Oxford. doi: 10.1016/B0-08-042993-9/00069-3.
[3] Fllyin F, Rohrbacher C. The influence of aqueous environment, temperature and cyclic loading on glass-fibre/epoxy composite laminates. J Reinforced Plastics Compos 2003;22(7):615–35. http://dx.doi.org/10.1177/073168403027609.
[4] Sanders B, editor. Characterization and failure analysis of plastics. Materials Park, OH: ASM International; 2004.
[5] Ray BC. Effects of changing environment and loading speed on mechanical behavior of FRP composites. J Reinf Plast Compos 2006;25(12):1227–40. http://dx.doi.org/10.1177/0731684406059783.
[6] Sethi S, Ray BC. Environmental effects on fibre reinforced polymeric composites: evolving reasons and remarks on interfacial strength and stability. Adv Colloid Interface Sci 2015;217:43–67. http://dx.doi.org/10.1016/j.cis.2014.12.005.
[7] Etches J, Potter K, Paul Weaver, Ian Bond. Environmental effects on thermally induced multi stability in unsymmetric composite laminates. Compos A: Appl Sci Manuf 2009;40(8):1240–7. http://dx.doi.org/10.1016/j.compositesa.2009.05.018.
[8] Yu Q, Chen P, Gao Y, Mu J, Chen Y, Lu C, et al. Effects of vacuum thermal cycling on mechanical and physical properties of high performance carbon/bismaleimide composite. Mater Chem Phys 2011;130(3):1046–53. http://dx.doi.org/10.1016/j.matchemphys.2011.08.033.
[9] Shin KB, Kim CG, Hong CS, et al. Prediction of failure thermal cycles in graphite/epoxy composite materials under simulated low earth orbit environments. Compos Part B 2000;31(3):223–35. http://dx.doi.org/10.1016/S1359-8368(99)00073-6.
[10] Ghasemi AR, Moradi M. Low thermal cycling effects on mechanical properties of laminated composite materials. Mech Mater 2016;96:126–37. http://dx.doi.org/10.1016/j.mechmat.2016.01.012.
[11] Pettermann HE, Desimone A. An anisotropic linear thermo-viscoelastic constitutive law. Mech Time-Dependent Mater 2017;2:1–13. http://dx.doi.org/10.1007/s11043-017-9364-x.
[12] Mcclure G, Mohammadi Y. Compression creep of pultruded E-glass-reinforced-plastic angles. J Mater Civ Eng 1995;7(4):269–76. http://dx.doi.org/10.1061/(ASCE)0899-1561(1995) 7:4(269).
[13] Sá MF, Gomes AM, Correia JR, et al. Creep behavior of pultruded GFRP elements – Part 1: Literature review and experimental study. Compos Struct 2011;93(10):2450–9. http://dx.doi.org/10.1016/j.compstruct.2011.04.013.
[14] Scott DW, Zureick AH. Compression creep of a pultruded e-glass/vinylester composite. Compos Sci Technol 1998;98(8):1361–9. http://dx.doi.org/10.1016/S0266-3538(98)00009-8.
[15] Shao Y, Shanmugam J. Deflection creep of pultruded composite sheet piling. J Compos Constr 2004;8(8):471–9. http://dx.doi.org/10.1061/(ASCE)1090-0268(2004) 8:5(471).
[16] Petermann J, Schulte K. The effects of creep and fatigue stress ratio on the long-term behaviour of angle-ply CFRP. Compos Struct 2002;57(1–4):205–10. http://dx.doi.org/10.1016/S0263-8223(02)00084-3.
[17] Goertzen WK, Kessler MR. Creep behavior of carbon fiber/epoxy matrix composites. Mater Sci Eng A 2006;421(1):217–25. http://dx.doi.org/10.1016/j.msea.2006.01.063.
[18] Ascione L, Berardi VP, D'Aponte A. Creep phenomena in FRP materials. Mech Res Commun 2012;43:15–21. http://dx.doi.org/10.1016/j.mechrescom.2012.03.010.
[19] Mancusi G, Spadea S, Berardi VP. Experimental analysis on the time-dependent bonding of FRP laminates under sustained loads. Compos Part B Eng 2013;46(2):116–22. http://dx.doi.org/10.1016/j.compositesb.2012.10.007.
[20] Ascione L, Berardi VP, Giordano A, et al. Local buckling behavior of FRP thin-walled beams: a mechanical model. Compos Struct 2013;98(3):111–20. http://dx.doi.org/10.1016/j.compstruct.2012.10.049.
[21] Ascione L, Berardi VP, Giordano A, et al. Buckling failure modes of FRP thin-walled beams. Compos Part B 2013;47(3):357–64. http://dx.doi.org/10.1016/j.compositesb.2012.11.006.
[22] Bottoni M, Mazzotti C, Savoia M. Creep tests on GFRP pultruded specimens subjected to traction or shear. Compos Struct 2014;108(108):514–23. http://dx.doi.org/10.1016/j.compstruct.2013.09.057.
[23] Boscato G, Casalegno C, Russo S. Creep effects in pultruded FRP beams. Mech

Compos Mater 2016;52(1):27–42.
[24] Yanes-Armas S, Castro JD, Keller T. Long-term design of FRP-PUR web-core sandwich structures in building construction. Compos Struct 2017:1–181. http://dx.doi.org/10.1016/j.compstruct.2017.08.089.
[25] GB/T 1456-2005, Test method for flexural properties of sandwich construction. Beijing: Standards Press of China.
[26] GB/T 1449-2005, Fibre-reinforced plastic composites—determination of flexural properties, Beijing: Standards Press of China.
[27] MIL-HDBK-17-1F, Composite Materials Handbook, Vol 1. Polymer Matrix Composites Guidelines for Characterization of Structural Materials, Department of Defense, USA.
[28] GB/T 11546.1-2008, Plastic—determination of creep behaviour—Part 1: Tensile creep, Beijing: Standards Press of China.
[29] Gibson RF. Principles of composite material mechanics. Boca Raton: CRC Press; 2016.
[30] Drozdov AD, Lejre ALH. Viscoelasticity, viscoplasticity, and creep failure of polypropylene/clay nanocomposites. Compos Sci Technol 2009;69(15):2596–603. http://dx.doi.org/10.1016/j.compscitech.2009.07.018.
[31] Biswas KK, Somiya S, Endo J. Creep behavior of metal fiber-PPE composites and effect of test surroundings. Mech Time-Dependent Mater 1999;3(1):85–101. http://dx.doi.org/10.1023/A:100984750688.
[32] Sakai T, Somiya S. Analysis of creep behavior in thermoplastics based on viscoelastic theory. Mech Time-Dependent Mater 2011;15(3):293–308. http://dx.doi.org/10.1007/s11043-011-9136-y.
[33] Hartmann B, Haque MA. Equation of state for polymer solids. J Appl Phys 1985;58(8):2831–6. http://dx.doi.org/10.1063/1.335881.
[34] Findley WN. Mechanism and mechanics of creep of plastics. SPE J 1960;16(1):57–65.